Applied Catalysis B: Environmental 259 (2019) 118066

Contents lists available at ScienceDirect

Applied Catalysis B: Environmental

journal homepage: www.elsevier.com/locate/apcatb

Ambient-temperature catalytic degradation of aromatic compounds on iron oxide nanorods supported on carbon nanofiber sheet

Yiseul Park[a,1], Chuhyung Kim[b,1], Minsun Kim[c], Soonhyun Kim[c], Wonyong Choi[b,*]

[a] Department of Chemical Engineering, Pukyong National University, Busan, 48513, Republic of Korea
[b] Department of Chemical Engineering & Division of Environmental Science and Engineering, Pohang University of Science and Technology (POSTECH), Pohang, 37673, Republic of Korea
[c] Smart Textile Convergence Research Group, Daegu Gyeongbuk Institute of Science and Technology (DGIST), Daegu, 42988, Republic of Korea

ARTICLE INFO

Keywords:
Iron oxide nanorods
Carbon nanofibers
Ambient temperature catalytic oxidation
Reactive oxygen species (ROS) generation
Advanced oxidation process (AOP)

ABSTRACT

Fe_2O_3 nanorods loaded on carbon nanofiber sheet (Fe_2O_3/CNF) was found to be active in degrading aromatic pollutants spontaneously under the dark and ambient conditions without using any chemical reagent or external energy to assist the degradation reaction. The removal of aromatic pollutants was not caused by adsorption but by oxidative degradation since the generation of degradation intermediates and products was observed. The Fe_2O_3/CNF exhibited selective degradation activities for aromatic-compounds. Degradation was induced by Fe_2O_3/CNF only, whereas neither iron oxide nor bare CNF alone exhibited any degradation activity. The degradation on the Fe_2O_3/CNF was enabled only in the presence of dissolved O_2 of which reduction led to the generation of reactive oxygen species (ROS). It is proposed that electrons spontaneously transfer from aromatic-compound to O_2 viaFe_2O_3/CNF with initiating the oxidative degradation and the concurrent ROS generation. The direct electron transfer from organic compound to Fe_2O_3/CNF, which lead to oxidative degradation.

1. Introduction

Iron oxide is an abundant and environmentally benign material, which has been extensively investigated for its applications to environmental remediation processes such as photocatalysis [1,2], photoelectrochemistry [3,4], and Fenton reaction [5–7]. However, the successful removal of various pollutants using an iron oxide material requires either external energy (*e.g.,* light, and electricity) or chemical reagents (*e.g.,* H_2O_2), which increases the process cost and limits practical applications. Therefore, these applications require the development of iron oxide-based catalysts that can remove pollutants under dark and ambient conditions without the use of external stimulants. Recently, Fe/Fe_2O_3 composites have been used to degrade pollutants viaa reductive or oxidative pathway under dark conditions without additional reagents, but catalyst reuse and recovery were limited because of low catalytic property and stability [8–11]. The $SrFeO_{3-\delta}$ compound also degraded organic pollutants under dark and ambient conditions without external stimulants. However, it required a very high temperature (1200 °C) and a long time (24 h) for catalyst preparation and the catalyst stability was unknown [12]. The ZnO_2/polypyrrole composite has also been used for dye degradation under dark conditions without chemical oxidants. The initiation of this reaction, however, still required an external heat source (80 °C) [13].

This study proposes a hybrid catalyst system that consists of iron oxide and CNF, which enables the spontaneous oxidation of organic compounds under dark and ambient conditions without any external energy or chemical reagent. The Fe_2O_3/CNF composite was prepared by growing the nanorod-shaped iron oxide on CNF sheets using an electrochemical deposition method. Although the composites of iron oxide and carbon materials (*e.g.,* activated carbon, graphene, and graphene oxide) have been often used to remove pollutants, most composites are activated by light irradiation and/or H_2O_2 addition. Without light or H_2O_2, pollutants are removable only by adsorption on the surface of composite [14–17]. To our knowledge, this is the first study to report that the degradation of organic pollutants on iron oxide-based composites is possible under dark and ambient conditions without the need of light irradiation and/or H_2O_2. The Fe_2O_3/CNF catalysts were comprehensively characterized and the ambient catalytic oxidation reactions were investigated systematically to understand the overall degradation mechanism.

* Corresponding authors.
E-mail addresses: sh2358@dgist.ac.kr (S. Kim), wchoi@postech.edu (W. Choi).
[1] These authors contributed equally to this work and should be considered co-first authors.

https://doi.org/10.1016/j.apcatb.2019.118066
Received 12 June 2019; Received in revised form 5 August 2019; Accepted 6 August 2019
Available online 07 August 2019

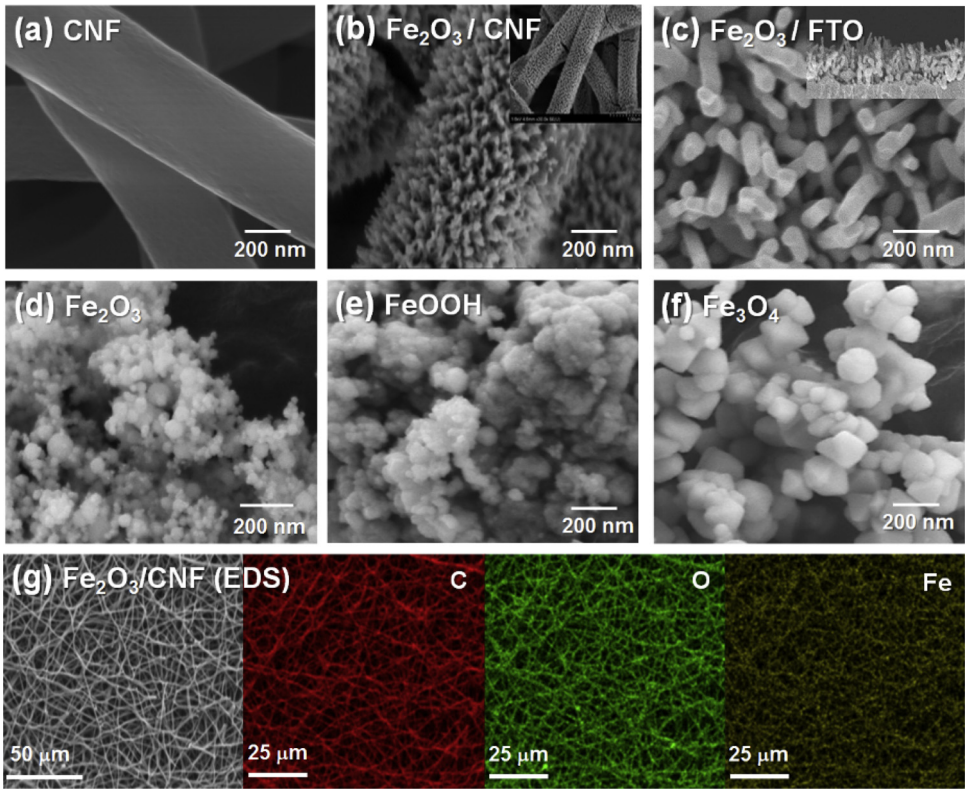

Fig. 1. SEM images of (a) bare CNF, (b) Fe_2O_3/CNF, (c) Fe_2O_3/FTO, and commercial iron oxides nanoparticles [(d) Fe_2O_3, (e) FeOOH, (f) Fe_3O_4], and (g) Fe_2O_3/CNF with the corresponding EDS elemental mapping images of C, O, and Fe.

2. Experimental details

2.1. Chemical reagents

The following chemicals were purchased from Sigma-Aldrich and used as received: polyacrylonitrile (PAN, M_w = 150,000), N,N-dimethylformamide (DMF), iron (II) sulfate heptahydrate ($FeSO_4{\cdot}7H_2O$), FeOOH, Fe_2O_3, Fe_3O_4, iron (III) chloride hexahydrate ($FeCl_3 \cdot 6H_2O$), sodium nitrate ($NaNO_3$), hydrochloric acid (HCl, 37%), sodium fluoride (NaF), terephthalic acid (TA), 4-chlorophenol (4-CP), catechol, phenol, acetaminophen (AP), carbamazepine (CP), 4-nitrophenol (4-NP), 4-chloroaniline (4-CA), acid orange 7 (AO7), benzoic acid (BA), ethylenediaminetetraacetic acid disodium salt (EDTA), 4-chlorocatechol (4-CC), hydroquinone (HQ), hydroxyhydroquinone (HHQ), sodium dichloroacetate (DCA), sodium arsenite ($NaAsO_2$,(As(III)), molybdate reagent solution (Fluka Analytical), ascorbic acid (AA), *tert*-butanol (TBA), superoxide dismutase from bovine erythrocytes (SOD), hydrogen peroxide (H_2O_2, ≥ 30%), peroxidase from horseradish (POD), N,N-diethyl-p-phenylenediamine (DPD), 5,5-dimethyl-1-pyrroline-N-oxide (DMPO), sodium bicarbonate ($NaHCO_3$), sodium carbonate (Na_2CO_3), phosphoric acid (H_3PO_4), acetonitrile (CH_3CN), and sodium perchlorate ($NaClO_4$). Deionized water (> 18 MΩ•cm) produced by a Barnstead purification system was used to prepare suspensions in all experiments.

2.2. Carbon nanofiber (CNF) sheet preparation

CNF sheets were prepared using an electrospinning technique. The initial stages of production for each CNF sheet involved the preparation for 10 wt.% PAN solution by dissolving PAN in DMF solvent and heating the mixture at 85 °C while stirring for 4 h. This was followed by cooling to room temperature for another 12 h with stirring. The viscous PAN solution was subsequently placed in a hypodermic syringe, which was positioned at a fixed distance (12 cm) from a metal cathode (collector). A dense web of the PAN nanofibers was then collected under an applied potential of 20 kV (eS-robot, NanoNC Co., Ltd.) and carbonized in a tube furnace with a N_2 flow to produce the CNF sheets. The carbonization process consisted of the following steps: (i) the stabilization of the PAN nanofibers in air at a temperature of 250 °C for 20 min, (ii) subsequent carbonization of the PAN nanofibers at 750 °C for 1 h with a N_2 flow, and (iii) heating the PAN nanofibers at 1400 °C for 1 h with a N_2 flow.

2.3. Fe_2O_3/CNF preparation

Fe_2O_3/CNF was prepared using the electrodeposition method reported in our previous study [18]. The conductive property of CNF allows its use as a substrate in iron oxide electrodeposition. The deposition was performed in an undivided cell using a Versastat 3 potentiostat (Princeton Applied Research). A typical three-electrode system composed of a CNF working electrode, an Ag/AgCl (4 M KCl) reference electrode, and a Pt wire counter electrode was used. FeOOH was deposited on the CNF immersed in an aqueous solution of 0.1 M $FeSO_4$ by anodic electrodeposition at 1.2 V (*vs.* Ag/AgCl) and 70 °C until 500 C of charge had passed through 1 g of CNF (500 C g^{-1}). Under these conditions, Fe^{2+} ions were electrochemically oxidized to Fe^{3+} ions, which were precipitated as FeOOH on the CNF surfaces. The FeOOH/CNF composite was converted into the Fe_2O_3/CNF composite by annealing at 400 °C for 4 h in air (*i.e.,* at a heating rate of 1 °C min^{-1}). The annealing temperature is limited to 400 °C in the presence of air to prevent CNF decomposition into CO_2.

Fe_2O_3/FTO as a control material was synthesized by previously reported hydrothermal method [19]. FTO as a substrate was vertically aligned in a Teflon tube containing an aqueous solution of $FeCl_3 \cdot 6H_2O$ and $NaNO_3$. The above solution was acidified by dropping HCl to prevent iron precipitation. The Teflon tube was placed in a stainless steel reactor and kept in an oven at 100 °C for 6 h and cooled to room temperature. The resulting sample (FeOOH/FTO) was rinsed with ultrapure

water and dried at room temperature, then annealed at 550 °C for 1 h and at 800 °C for 20 min to obtain Fe_2O_3/FTO. The mass fraction of Fe_2O_3 in the Fe_2O_3/FTO composite was approximately 11%. We also prepared Fe_2O_3/FTO using the electrodeposition method as in the preparation of Fe_2O_3/CNF but it did not produce the rod structure of Fe_2O_3. Therefore, Fe_2O_3/FTO prepared by the hydrothermal method was compared with Fe_2O_3/CNF sample since both samples are similar in the iron oxide morphology (*see* Fig. 1).

2.4. Catalysts characterization

Surface morphology images were obtained using a field emission scanning electron microscope (FE-SEM, Hitachi S4-8020). The thermogravimetric (TGA) measurements were performed on the composites using an SDT Q600 system (TA Instruments). X-ray diffraction (XRD) patterns were obtained using an X-ray diffractometer (Panalytical, Empyrean, 40 kV, 30 mA) with Cu-Kα_1 radiation (λ = 1.54178 Å) and a quartz monochromator. Finally, the elemental states in the composites were determined using an ESCALAB 250xi X-ray photoelectron spectroscopy (XPS) system with Mg–Kα radiation (1253.6 eV). All XPS spectra were calibrated with respect to the C 1s peak (285 eV), and all X-ray absorption near-edge structure (XANES) experiments were conducted at 8C nano XAFS beamline of Pohang Light Source-II. The dissolved iron concentrations were measured using Inductively Coupled Plasma optical emission spectrometry (ICP-OES-6300, Thermo scientific). The specific surface area was obtained by N_2 adsorption measurements on a Mirae SI nanoporosity-XQ analyzer by the Brunauer-Emmett-Teller (BET) method. Diffuse reflectance UV-vis absorption spectra (DRS) were obtained by using a UV-vis spectrophotometer (Shimadzu UV-2600) with an integrating sphere attachment and $BaSO_4$ was used as the reference.

2.5. Reactivity analysis methods

For the degradation tests, CNF-based samples (CNF, FeOOH/CNF, and Fe_2O_3/CNF) were immersed in an aqueous solution containing a test substrate (*i.e.,* phenol, 4-CP, AP, CP, catechol, 4-NP, 4-CA, AO7, BA, DCA, EDTA, or As(III)). Equal sample aliquots were withdrawn from the reactor intermittently. The degradation of 4-CP and the production of 4-CC were monitored by using a high performance liquid chromatography (HPLC, Agilent 1100 series) equipped with a diode array detector and a ZORBAX 300SB-C18 column (4.6 mm × 150 mm). The binary mixture, consisting of a 0.1% of aqueous phosphoric acid and acetonitrile (70:30 v/v) solution, was used as a mobile phase. The production of Cl^- and CO_2 was monitored using an ion chromatograph (IC, Dionex DX-120) with an eluent composed of 3.5 mM Na_2CO_3 and 1 mM $NaHCO_3$ and a gas chromatograph (GC, HP6890, Agilent), respectively. The removal of the total organic carbon (TOC) was monitored using a TOC analyzer (Shimadzu TOC-V_{SH}).

For the multi-activity assessment test, the concentrations of aromatic compounds (*i.e.,* phenol, 4-CP, AP, CP, catechol, 4-NP, 4-CA, and BA) and EDTA were monitored by using HPLC. DCA and AO7 were quantified by using IC and UV-vis spectrophotometer, respectively. As (III) was determined by a colorimetrical method using molybdenum blue as a reagent. Absorbance measurements were performed at 870 nm (ε = 19550 $M^{-1}\,cm^{-1}$) using a UV-vis spectrophotometer. Furthermore, the concentration of H_2O_2 was determined by using a DPD colorimetric method (based on the horseradish peroxidase-catalyzed reaction between H_2O_2 and DPD) using a UV-vis spectrophotometer (λ_{max} = 551 nm, ε = 21,000 M^1 cm) [20]. For electron paramagnetic resonance (EPR) analysis, DMPO was employed as a spin-trapping reagent for •OH and $O_2^{\bullet-}$. The EPR spectra of Fe_2O_3/CNF were obtained using a JEOL JES-X310 spectrometer at the following conditions: center field = 335 mT; microwave frequency = 9.415 GHz; microwave power = 1.00 mW; modulation frequency = 100 kHz; and modulation width = 0.2 mT. Anodic current generation was monitored at a chronoamperometry condition using a potentiostat (Versastat 3). Fe_2O_3/CNF was used as the working electrode (WE), and Pt wire and Ag/AgCl were used as the counter and the reference electrode, respectively. 0.1 M $NaClO_4$ solution was used as the base electrolyte. Before the addition of 4-CP, the open circuit potential of Fe_2O_3/CNF was monitored until its stabilization. The stabilized open circuit potential was applied to collect currents and then an aliquot of 4-CP solution (10 mM) was spiked during the current measurement of the Fe_2O_3/CNF.

3. Results and discussion

3.1. Physicochemical properties of the Fe_2O_3/CNF

The morphologies of bare CNF, Fe_2O_3/CNF, and Fe_2O_3/FTO were examined by SEM (Figs. 1a-c). The smooth surface of the bare CNF was uniformly covered with Fe_2O_3 nanorods that have the diameter of ~10 nm and the average length of ~150 nm. The element mapping images clearly confirmed the uniform distribution of Fe_2O_3 on CNF surface (Fig. 1g). For the comparison, the Fe_2O_3 nanorods were grown onto the FTO electrode using a simple hydrothermal method [19]. The diameter and average length of Fe_2O_3 nanorods were around 50 nm and 750 nm, respectively. The average particle sizes of commercial iron oxides (*i.e.,* Fe_2O_3, FeOOH, and Fe_3O_4) used for the comparison of activity were 10–200 nm (Figs. 1–f).

Fig. 2a shows the comparison of XRD patterns of CNF, FeOOH/CNF, and Fe_2O_3/CNF. The peaks in the Fe_2O_3/CNF sample match the standard α-Fe_2O_3 diffraction peaks (blue lines, JCPDS Card No. 33-0664). A small portion of FeOOH may have remained in the Fe_2O_3/CNF sample because of the incomplete conversion of FeOOH to Fe_2O_3. Fig. 2b shows the TGA curve of Fe_2O_3/CNF. The weight loss observed at a temperature range of 400–600 °C was attributed to thermal decomposition of the CNF, and the stable residue that formed at temperatures greater than 600 °C is attributed to Fe_2O_3. According to the TGA result of Fe_2O_3/CNF, the mass fraction of Fe_2O_3 in the Fe_2O_3/CNF composite was approximately 30%. The XPS Fe 2p and O 1s spectra of the Fe_2O_3/CNF were shown in Figs. 2c and d, respectively, and were compared with those of the commercial Fe_2O_3 nanopowder samples. The Fe $2p_{3/2}$ peak binding energy (BE) of the Fe_2O_3/CNF was 710.78 eV, which is slightly different compared with the commercial Fe_2O_3 nanoparticle. The small differences between the prepared Fe_2O_3/CNF samples and references are ascribed to different preparation methods. In addition, it is possible that Fe_2O_3/CNF contained a small amount of unconverted FeOOH in the composite resulting in a slight peak shift. On the other hand, the XPS O 1s spectra of the prepared Fe_2O_3/CNF sample exhibited significantly different shapes compared with the spectra of the reference Fe_2O_3 nanoparticle. Both of the Fe_2O_3/CNF and reference samples show a peak at 529.8 eV, which corresponds to the lattice oxygen species, but only Fe_2O_3/CNF exhibited the second peak at 531.5 eV, which is assigned as the lattice OH or adsorbed OH [21]. Considering that the peak at 531.5 eV is also observed as a main peak in the spectra of FeOOH/CNF and FeOOH, the peak at 531.5 eV in Fe_2O_3/CNF can be attributed to the presence of FeOOH and the surface OH groups on Fe_2O_3. The deconvolution of the XPS spectra of Fe 2p and O 1s for Fe_2O_3/CNF sample was done in agreement with the data given in the reference (Fig. S1) [21–23]. Typically, the XPS spectrum of Fe $2p_{3/2}$ was fitted with multiplet split spectra due to its complexity induced by unpaired electrons in Fe atom [23]. The deconvoluted spectra's binding energies (BE) and the full width at half maximum (FWHM) well matched those of multiplets in Fe_2O_3 references, which are summarized in Table S1. The specific surface area of Fe_2O_3/CNF was measured to be 193 m^2/g by Brunauer-Emmett-Teller (BET) method.

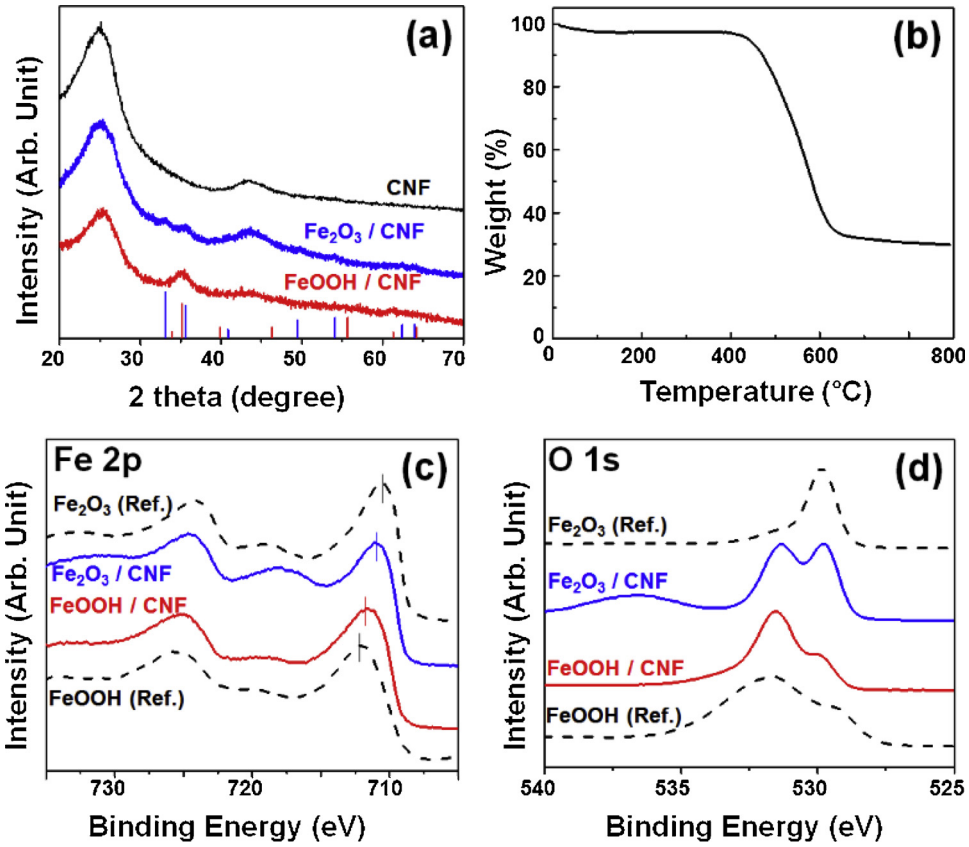

Fig. 2. Characterizations of the prepared catalysts. (a) XRD patterns of CNF, FeOOH/CNF, and Fe_2O_3/CNF, (b) The TGA curve of the Fe_2O_3/CNF, (c) XPS Fe 2p, and (d) XPS O 1s spectra of FeOOH/CNF (red), Fe_2O_3/CNF (blue), and references (Fe_2O_3, and FeOOH) (For interpretation of the references to colour in this figure legend, the reader is referred to the web version of this article).

3.2. Degradation of 4-CP as the main test substrate under the dark and ambient conditions

The catalytic activity of Fe_2O_3/CNF was measured and compared with those of bare CNF, commercial iron oxides nanoparticles, FeOOH/CNF, and Fe_2O_3/FTO with respect to 4-CP degradation under dark condition (Fig. 3a). The Fe_2O_3/CNF samples (2 g L^{-1} containing 30 wt.% iron oxide) and Fe_2O_3/FTO electrode (1.2 g L^{-1}; based on the amount of Fe_2O_3 on Fe_2O_3/FTO) were immersed in 4-CP solution, whereas the commercial iron oxides nanoparticles (1.2 g L^{-1}) were suspended with stirring in 4-CP solution. Nearly 80% of 4-CP removal was achieved in 6 h with Fe_2O_3/CNF without the need of external energy and chemical oxidants whereas the degradation of 4-CP was negligible in the presence of bare CNF, commercial iron oxides nanoparticles, FeOOH/CNF, and Fe_2O_3/FTO. It should be noted that the commercial iron oxides nanoparticles have widely varying sizes (*ca.* 10–200 nm, Figs. 1–f) but none of them exhibited any measurable activity for 4-CP oxidation. This implies that iron oxide nanoparticles alone are not reactive at all regardless of their sizes. The Fe_2O_3 grown on FTO also has a similar rod-like structure (Fig. 1c) as Fe_2O_3/CNF, but it does not exhibit any activity. The unique oxidation activity of Fe_2O_3/CNF, which clearly distinguishes itself from bare CNF, commercial iron oxide nanoparticles, and Fe_2O_3/FTO, seems to be little related with the size and structure of Fe_2O_3 itself. The abnormal reactivity of Fe_2O_3 is induced only when Fe_2O_3 is loaded on CNF, which implies that the presence of interfacial junction between Fe_2O_3 and CNF is critical in inducing the reactivity.

Fig. 3b shows the generation of chloride ions (Cl^-) and 4-CC (as a product and an intermediate, respectively) during 4-CP degradation on Fe_2O_3/CNF. A higher 4-CP (100 μM) concentration and longer reaction time (24 h) were employed in this experiment to allow the determination of intermediates and products. Although the significant deficit in the Cl mass balance indicates that there are a number of missing products and intermediates (Fig. S2), the apparent generation of Cl^- and 4-CC indicates that the observed 4-CP removal on Fe_2O_3/CNF did not occur viaasimple adsorption but by the 4-CP degradation. Furthermore, the generation of CO_2 during 4-CP degradation on Fe_2O_3/CNF also confirmed 4-CP mineralization. The amount of generated CO_2 in a closed reactor headspace was analyzed by using GC. This reactor was purged with O_2 or N_2 gas for 30 min prior to the reaction. The generation of CO_2 on bare CNF and Fe_2O_3/CNF in the absence of 4-CP was monitored for 3 h prior to 4-CP introduction, which showed no signs of CO_2 generation without 4-CP (Fig. 3c). When an aliquot of the 4-CP solution was spiked into the reactor, both 4-CP degradation and CO_2 generation were immediately observed in the O_2 saturated solution with Fe_2O_3/CNF, which indicates the occurrence of 4-CP mineralization. Although 70% of 4-CP was removed on Fe_2O_3/CNF (w/ O_2) in 6 h, the quantification of CO_2 (~30 μM) indicates that only 25% of the removed 4-CP was slowly mineralized. TOC removal also confirmed the mineralization process, and we observed that ~25% of the TOC was removed after 6 h, which is consistent with the yield of CO_2 generation. However, when the degradation of 4-CP on Fe_2O_3/CNF was performed in N_2 saturated condition, where the oxidant generation viaO_2 reduction is not possible, the removal of 4-CP and the production of CO_2 were both negligible. This indicates that dissolved O_2 is an essential oxidant precursor responsible for the degradation of 4-CP. In addition, it is noted that the degradation of 4-CP on Fe_2O_3/CNF was accelerated at the higher temperature (25 °C *vs.* 50 °C) as shown in Fig. S3, which indicates that the catalytic oxidation reaction proceeds faster at elevated temperature. This also reconfirms that the removal of 4-CP should not be an adsorption process since higher temperature should hinder its adsorption.

3.3. Spontaneous ROS generation on Fe_2O_3/CNF

To investigate the oxidation mechanism that occur on Fe_2O_3/CNF, several reactive oxygen species (ROS, *i.e.,* •OH, and $O_2^{\bullet-}$) scavengers were added during 4-CP degradation (Fig. 4). The presence of TBA as a •OH scavenger decelerated (~66%) the degradation of 4-CP, which

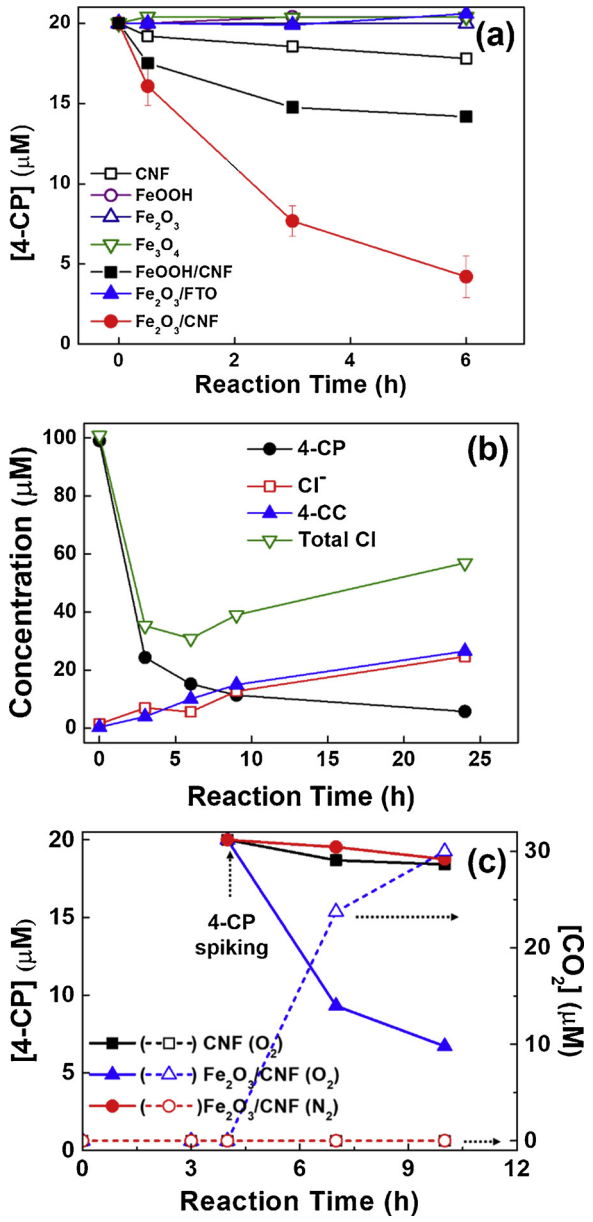

Fig. 3. (a) Time-profiles of 4-CP (C_0 = 20 μM) degradation with different catalysts under dark conditions, [CNF, FeOOH/CNF, and Fe_2O_3/CNF] = 2 g L^{-1}, and [powder samples and Fe_2O_3/FTO] = 1.2 g L^{-1}. (b) The production of chloride ions (Cl^-)and 4-CC from 4-CP (C_0 = 100 μM) degradation on Fe_2O_3/CNF (4 g L^{-1}; Total Cl = [4-CP] + [4-CC] + [Cl]). (c) 4-CP (C_0 = 20 μM) degradation and the concurrent CO_2 generation on bare CNF and Fe_2O_3/CNF in O_2 and N_2 saturated solutions. 4-CP was spiked into the reactor after 3.5 h of blank testing (without 4-CP).

implies that the production of •OH on Fe_2O_3/CNF. The addition of SOD, which quenches the $O_2^{\bullet-}$ (an intermediate for the generation of •OH), also decreased the rate of 4-CP degradation by approximately 45%. However, the fact that the addition of TBA and SOD did not completely inhibit 4-CP degradation implies that the direct oxidation of 4-CP on Fe_2O_3/CNF is an alternative degradation pathway.

The generation of •OH during 4-CP degradation on the Fe_2O_3/CNF was monitored by using TA as a selective probe reagent for •OH trapping (Fig. 5a). The reaction of TA with •OH produces 2-hydroxyterephthalic acid (2-HTA), and the generation of 2-HTA can be monitored by measuring its fluorescence emission (λ_{ex} = 315 nm) [24]. Fe_2O_3/CNF produced 2-HTA during 4-CP degradation and suggests that the generation of •OH as a main oxidant is responsible for the catalytic

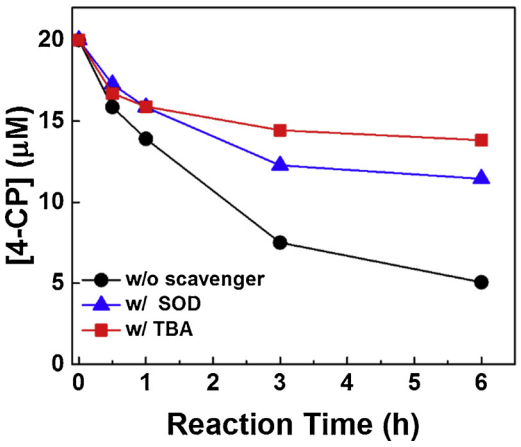

Fig. 4. The effects of the superoxide (SOD) and OH radical scavenger (TBA) on 4-CP degradation on Fe_2O_3/CNF samples. $[4\text{-CP}]_0$ = 20 μM, $[Fe_2O_3/CNF]$ = 2 g L^{-1}, and $[SOD]_0$ = $[TBA]_0$ = 50 mg L^{-1}.

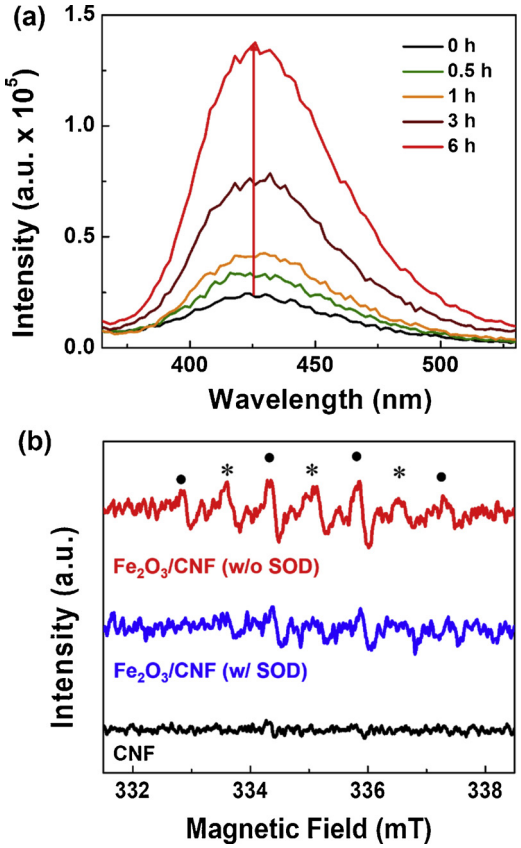

Fig. 5. (a) Fluorescence emission spectra evolution as a result of hydroxylated product formation via•OH reaction with TA (•OH probe reagent) on Fe_2O_3/CNF. $[4\text{-CP}]_0$ = 20 μM, $[Fe_2O_3/CNF]$ = 2 g L^{-1}, and $[TA]_0$ = 50 μM in 2 mM of NaOH. (b) Spin trap EPR experiments of CNF and Fe_2O_3/CNF in the suspension of 4-CP with or without SOD, (•): DMPO − OH adducts, (*): DMPO − OOH adducts, $[4\text{-CP}]_0$ = 20 μM, [CNF and Fe_2O_3/CNF] = 5 g L^{-1}, $[SOD]_0$ = 50 mg L^{-1}, and [DMPO] = 30 mM.

oxidation activity of Fe_2O_3/CNF. Incidentally, it is interesting to note that 2-HTA was not generated on Fe_2O_3/CNF in the absence of 4-CP, which suggests that the organic substrate compound (4-CP in this case) plays an important role in •OH generation.

Using the EPR spin-trapping technique, we detected oxidizing radicals such as •OH and $O_2^{\bullet-}$ in 4-CP solution in the presence of Fe_2O_3/CNF, which is shown in Fig. 5b. Typical DMPO − OH(•) and

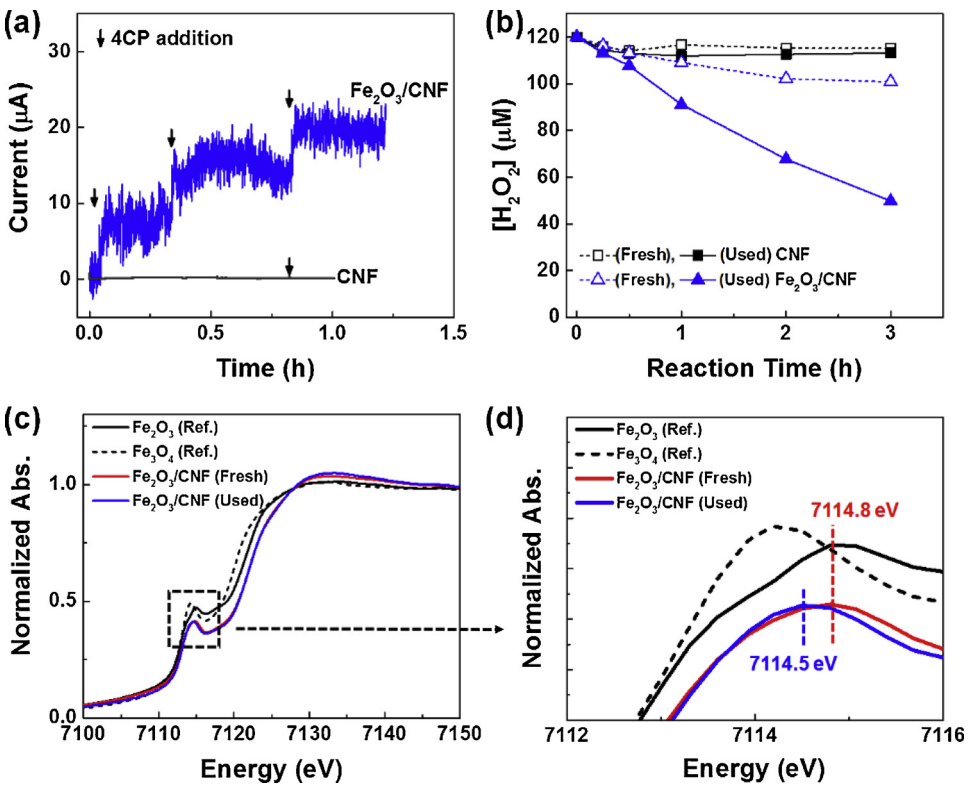

Fig. 6. Proofs of the direct electron transfer between 4-CP and Fe_2O_3/CNF. (a) current change upon adding 4-CP (10 mM, 0.3 mL) onto the CNF and Fe_2O_3/CNF electrode. Electrolyte: 30 mL of 0.1 M $NaClO_4$. (b) H_2O_2 decomposition on the fresh Fe_2O_3/CNF sample and the used Fe_2O_3/CNF sample (recovered after reaction with 4-CP). $[H_2O_2]_0$ = 120 μM, and [CNF and Fe_2O_3/CNF] = 0.5 g L^{-1}. The XANES spectra of (c) Fe_2O_3/CNF and (d) its magnified spectra of before and after the 4-CP degradation experiments.

DMPO − OOH(*) peaks were observed in the presence of Fe_2O_3/CNF, whereas no peaks were observed on bare CNF [25]. The peaks that are the characteristic of DMPO − OH and DMPO − OOH in the EPR spectra ensure the formation of •OH and $O_2^{\bullet -}$ during the 4-CP degradation reaction on Fe_2O_3/CNF. On the other hand, when SOD was added to the 4-CP solution with Fe_2O_3/CNF, the peak intensities corresponding to the DMPO − OH and DMPO − OOH were significantly decreased. It supports that •OH is generated via $O_2^{\bullet -}$ (or $HO_2^{\bullet}$) and is consistent with the finding that the presence of SOD inhibits 4-CP degradation (Fig. 4). Overall, these results corroborate that the Fe_2O_3/CNF spontaneously generated ROS under dark and ambient conditions.

3.4. Evidence for direct electron transfer on the Fe_2O_3/CNF

The direct electron transfer from 4-CP to the Fe_2O_3/CNF was confirmed by measuring current generation when an aliquot of the 4-CP solution (10 mM, 0.3 mL) was spiked into the electrochemical cell containing the Fe_2O_3/CNF anode (Fig. 6a). The addition of 4-CP into an electrolyte solution immediately generated an anodic current, which indicates that electrons were transferred from 4-CP to the Fe_2O_3/CNF electrode. On the other hand, the 4-CP-induced current generation on the bare CNF was negligible. This result is consistent with the 4-CP degradation experiment (*see* Fig. 3a). The electron transfer from 4-CP to the Fe_2O_3/CNF may reduce Fe species on Fe_2O_3/CNF. To test this possibility, we compared the decomposition of H_2O_2 by using fresh Fe_2O_3/CNF and the used Fe_2O_3/CNF (which was recovered after 4-CP degradation) in Fig. 6b. Since the decomposition of H_2O_2 by Fe^{2+} is much faster than the decomposition by Fe^{3+} ($k_{Fe^{2+}} = 76 \times 10^5$ M^{-1} s^{-1} *vs.* $k_{Fe^{3+}} = 0.002$ M^{-1} s^{-1}) [5,6], the accelerated decomposition of H_2O_2 on the Fe_2O_3/CNF might indicates the presence of Fe^{2+} species on the catalyst. The decomposition of H_2O_2 on the bare CNF was negligible regardless of whether the CNF was fresh or used. Whereas, the decomposition of H_2O_2 on the used Fe_2O_3/CNF was much faster than that of the fresh sample. It indicates that the formation of Fe^{2+} species on Fe_2O_3/CNF as a result of the electron transfer from organic substrate (*i.e.,* 4-CP) to the Fe_2O_3. Additionally, through XANES analysis further confirmed the difference of the oxidation states of Fe between the fresh and used Fe_2O_3/CNF in Fig. 6c. The pre-edge position is a sensitive indicator of the relative fraction of Fe^{2+} and Fe^{3+} and is shown in Fig. 6d [26,27]. The pre-edge positions of Fe_2O_3/CNF (Fig. 6d) after 4-CP degradation shifted to 7114.5 eV, which is the middle energy region between that of commercial Fe_2O_3 and Fe_3O_4. This result strongly demonstrates that the lower Fe oxidation state (*i.e.,* Fe^{2+}) was generated as a result of the organic substrate-induced reduction of Fe species on the Fe_2O_3/CNF composite.

The observation of the 4-CP induced electron transfer (current generation) on the Fe_2O_3/CNF electrode implies the presence of the surface interaction between 4-CP and the Fe_2O_3/CNF composite. The diffuse reflectance UV-vis spectra of 4-CP adsorbed Fe_2O_3/CNF provide evidence supporting the charge transfer interaction between them (*see* Fig. 7a). The adsorption of 4-CP on Fe_2O_3/CNF induced a broad absorption in the range of 350–600 nm, which indicates the presence of charge transfer interaction between 4-CP and Fe_2O_3/CNF. The adsorption of molecules (*e.g.,* phenolic compounds, EDTA, and cyanide) on metal oxide surface often induces the ligand-to-metal charge transfer (LMCT) [28,29], which is evidenced by the appearance of a visible-light absorption band despite the lack of visible light absorption by the adsorbate molecule itself. Therefore, the appearance of the visible light absorption band upon adsorbing 4-CP on Fe_2O_3/CNF supports the charge transfer interaction that should initiate the oxidation of the organic compounds. To further investigate the interactions between 4-CP and Fe_2O_3/CNF, fluoride ions (as NaF) which have a high adsorption affinity on the Fe_2O_3 surface [30,31] were added to the 4-CP solution to hinder the attractive interaction between 4-CP and the Fe_2O_3 surface (Fig. 7b). The addition of NaF significantly retarded 4-CP degradation, which indicates that adsorbed fluoride ions hinder the surface chemical interaction of 4-CP by occupying the active adsorption sites and subsequently retarded the electron transfer from 4-CP to Fe_2O_3/CNF. It confirms that the surface interaction between 4-CP and Fe_2O_3/CNF is essential for initiating the catalytic oxidation of 4-CP.

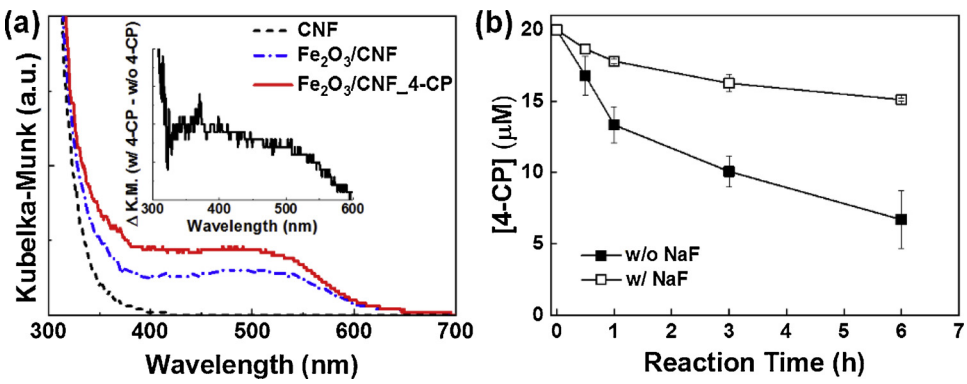

Fig. 7. (a) The diffuse reflectance UV-vis spectra (DRS) of bare CNF and Fe_2O_3/CNF with and without 4-CP adsorption. The inset shows the absorption difference spectrum between bare Fe_2O_3/CNF and 4-CP-adsorbed Fe_2O_3/CNF. (b) The effect of fluoride ions on the degradation of 4-CP on Fe_2O_3/CNF. $[4\text{-CP}]_0$ = 20 μM, $[Fe_2O_3/CNF]$ = 2 g L^{-1}, and [NaF] = 300 μM.

3.5. Substrate-specific catalytic activities of the Fe_2O_3/CNF and proposed mechanism

The pollutant degradation reactivity on the Fe_2O_3/CNF was strongly dependent on the type of pollutant. A variety of aromatic compounds (*i.e.,* phenol, 4-CP, AP, CP, catechol, 4-NP, 4-CA, AO7, and BA) and non-aromatic compounds (*i.e.,* DCA, EDTA, and As(III)) were used as a substrate for catalytic oxidation on the Fe_2O_3/CNF and the activities were compared in Fig. 8. Interestingly, we observed that only the aromatic compounds were degraded and the degradation of non-aromatic compounds on the Fe_2O_3/CNF was negligible. Considering that EDTA (non-aromatic compound) easily forms the surface complexes on metal oxide [28] and that EDTA should have a higher adsorption affinity than phenolic compounds on metal oxide surface, the strong surface adsorption on the Fe_2O_3/CNF does not seem to be a sufficient condition for effective catalytic oxidation of organic substrates. A clear explanation for the highly substrate-specific catalytic activity may need a more rigorous investigation to understand the phenomenon at the molecular level, which should be addressed in further studies. The proposed mechanism was discussed in the later part of this section.

The catalytic oxidation activity of the Fe_2O_3/CNF was verified by repeating the degradation reaction of 4-CP on Fe_2O_3/CNF in Fig. 9a. The degradation rates of 4-CP on Fe_2O_3/CNF gradually decreased over the course of repetitive reactions. The gradual deactivation of the composite catalyst can be ascribed to either the accumulation of degradation intermediates on the catalyst active sites or the loss of active species on the catalyst surface during the repeated reactions. For the confirmation of the Fe oxidation state after the repetitive reactions, Fe 2p XPS spectra of the fresh and used Fe_2O_3/CNF were compared as shown in Fig. 9b. It is noted that the maximum BE of Fe $2p_{3/2}$ peak was slightly shifted from 710.78 eV to 710.38 eV after the repetitive reactions. Since the Fe $2p_{3/2}$ peaks of Fe_2O_3 (Fe^{3+}) and FeO (Fe^{2+}) are centered at 710.8 eV and 709.6 eV, respectively, the Fe 2p spectra shift to the lower binding energy indicates the reduction of iron species in Fe_2O_3 during the repetitive reactions [22,32,33]. This partial reduction of Fe^{3+} after reactions might be related to the gradual decrease of reactivity of Fe_2O_3/CNF. Nevertheless, the morphology of Fe_2O_3/CNF did not exhibit any notable change with maintaining the nanorod structure even after the multi-cycles of repetitive reactions (Figs. 9c and d). To test the stability of the iron oxide, iron dissolution from the Fe_2O_3/CNF was measured using an ICP-OES after 4-CP degradation for 6 h (at $pH_i \approx 4$). The dissolved iron species from Fe_2O_3/CNF was approximately 40 ppb, which is negligible when compared with the total iron content in the composite catalyst sample. We can thus conclude that the Fe_2O_3/CNF has a stable composition and that the possible role of dissolved iron species in the observed oxidation process can be ruled out.

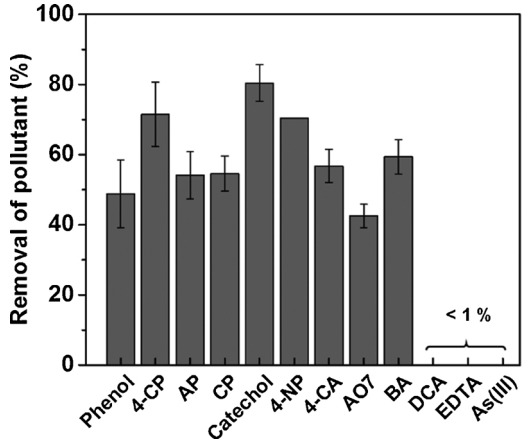

Fig. 8. The removal of aromatic compounds (*i.e.,* phenol, 4-CP, AP, CP, catechol, 4-NP, 4-CA, AO7, and BA) and non-aromatic compounds (*i.e.,* DCA, EDTA, and As(III)) on the Fe_2O_3/CNF after 6 h reactions. $[pollutants]_0$ = 20 μM, and $[Fe_2O_3/CNF]$ = 2 g L^{-1}.

On the basis of the above results and discussion, we suggest a catalytic degradation mechanism on the Fe_2O_3/CNF as illustrated in Scheme 1. The electron transfer was initiated from the aromatic compound (*i.e.,* 4-CP) to the Fe_2O_3/CNF, and the electrons were transferred to the CNF, and subsequently reduce O_2 to generate •OH viathe formation of $O_2^{\bullet -}$ and H_2O_2(Eqs. (1)–(4)). It is supposed that the direct interfacial contact between Fe_2O_3 and CNF should facilitate the spontaneous electron transfer from the aromatic molecule to the iron oxide and the CNF support along with the concurrent generation of ROS. The initial interaction between the aromatic compound and Fe_2O_3 seems to be mediated by cation (Fe^{3+})-π interaction as the following scheme.

$$\text{4-CP} \rightarrow \text{4-CP}^{\bullet +} + e^- \ (Fe_2O_3/CNF) \quad (1)$$

$$O_2 + e^- \ (Fe_2O_3/CNF) \rightarrow O_2^{\bullet -} \quad (2)$$

$$O_2^{\bullet -} + e^- + 2H^+ \rightarrow H_2O_2 \quad (3)$$

$$H_2O_2 + e^- + H^+ \rightarrow \bullet OH + H_2O \quad (4)$$

The degradation of 4-CP and the concurrent generation of intermediates were monitored by HPLC analysis, which confirmed the production of degradation intermediates such as hydroxyhydroquinone (HHQ), hydroquinone (HQ), and 4-chlorocatechol (4-CC) (*see* Fig. S2) [34,35]. The oxidative degradation of 4-CP has been extensively investigated in various advanced oxidation processes (AOPs) generating ROS and the above intermediates were commonly observed in the degradation process of 4-CP [36,37]. The fact that HHQ, HQ, and 4-CC (produced through the hydroxylation of 4-CP) were generated on the Fe_2O_3/CNF composite supports that •OH are involved in the degradation mechanism of 4-CP. The •OH induced reactions of 4-CP and its hydroxylated products further induce a ring cleavage, which leads to mineralization. It is consistent with the observation that Cl- and CO_2 were generated along with the degradation of 4-CP (*see* Figs. 3b and c).

Considering the fact that the oxidative degradation of organic substrates on the Fe_2O_3/CNF is limited to aromatic compounds (*see* Fig. 8),

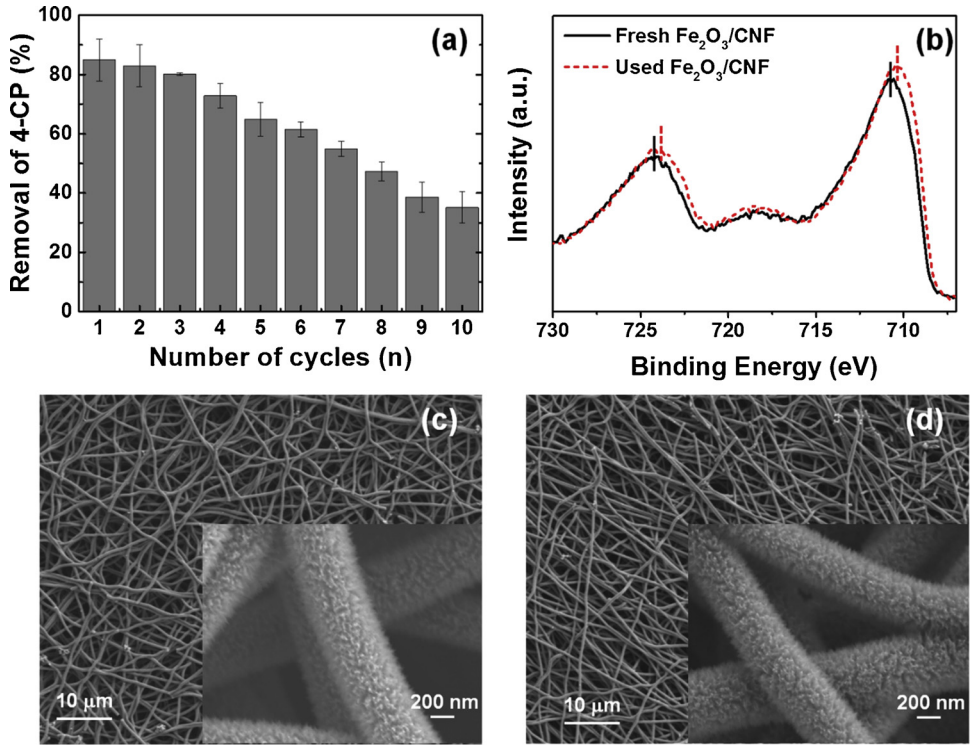

Fig. 9. (a) Activity variation of Fe_2O_3/CNF with the repeated cycles of 4-CP degradation. $[4\text{-CP}]_0$ = 20 μM, $[Fe_2O_3/CNF]$ = 2 g L^{-1}, and 6 h reaction, (b) Fe 2p XPS spectra of the fresh Fe_2O_3/CNF (solid lines) and used Fe_2O_3/CNF (dashed lines), (c) SEM images of the fresh Fe_2O_3/CNF and (d) used Fe_2O_3/CNF.

it seems that there is a specific interaction between aromatic compounds and the composite catalyst. It is postulated that the presence of aromatic π electrons plays an essential role in initiating the oxidative electron transfer from organic compounds to the Fe_2O_3/CNF. A plausible speculation is that the cationic-π interaction at the Fe^{3+} species located in the Fe_2O_3/CNF interfacial region is needed to initiate the subsequent electron transfer from the aromatic compound to iron oxide [38,39]. Aromatic compounds, which possess highly delocalized electrons, may act as an electron donor when interacting with electron-deficient species such as transition metal cations (*e.g.,* Fe^{3+}, and Cu^{2+}) [40]. Then, the electrons transferred from the aromatic compound to the iron oxide are transported through the conductive CNF support and subsequently transferred to O_2 to generate •OH via forming $O_2^{\bullet-}$ and H_2O_2. It should be noted that such spontaneous electron transfer was enabled only when the Fe_2O_3 and CNF were combined. Neither the commercial iron oxides nanoparticles nor bare CNF initiated the electron transfer. This indicates that the interfacial junction between the Fe_2O_3 and CNF may create a potential gradient that facilitates the spontaneous electron transfer.

The spontaneous electron transfer from an aromatic compound onto carbon nanomaterials (*e.g.,* carbon nanotube, and reduced graphene oxide) was similarly observed in the non-radical activation process of peroxymonosulfate (PMS) [41–44]. In the non-radical PMS activation, PMS acts as a strong oxidant (electron acceptor) that abstracts electrons from the organic substrate (aromatic compounds) through an electron transfer medium (*i.e.,* carbonaceous material, metal, and metal oxide) [43,44]. This spontaneous electron transfer process from an aromatic compound to PMS viacarbonaceous material can be similarly compared with that from an aromatic compound to O_2 viathe Fe_2O_3/CNF composite in this study. Another kind of spontaneous electron transfer from organic substance was also observed in the generation process of persistent free radical (PFR) on biochar/particulate materials (PM) derived from incomplete combustion [40,45–49]. Polyaromatic hydrocarbons (PAHs) produced from incomplete combustion transfer electrons to transition metal oxides (*i.e.,* Fe_2O_3, CuO, ZnO, and TiO_2) present in the carbon soot, which results in the generation of PFR, an oxidized PAH. PFR has a relatively long lifetime in the environment (lifetime ranging from minutes to months) because of highly delocalized π-electrons in

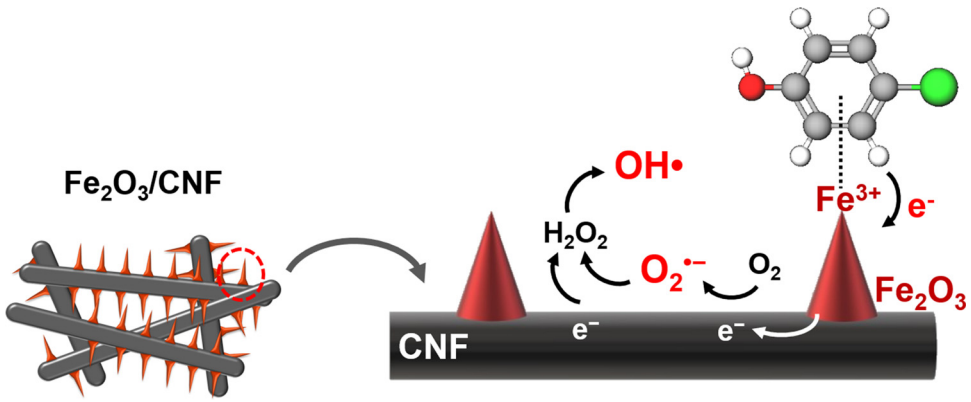

Scheme 1. Proposed 4-CP degradation mechanism on the Fe_2O_3/CNF composite under dark and ambient-temperature conditions. The direct interfacial contact between Fe_2O_3 and CNF should facilitate the spontaneous electron transfer from the aromatic molecule to the iron oxide and the CNF support along with the concurrent generation of ROS. The initial interaction between the aromatic compound and Fe_2O_3 seems to be mediated by cation (Fe^{3+})-π interaction.

the aromatic structure. The spontaneous electron transfer from PAH to carbonaceous soot material to generate PFR is conceptually similar to the present system where aromatic compounds transfer electrons to the Fe_2O_3/CNF to generate ROS. In this study, we found that such a spontaneous electron transfer can decompose aromatic compounds with the concurrent mineralization to CO_2 and ROS generation. This phenomenon can be employed as the mildest advanced oxidation process (AOP) that can decompose aquatic pollutants under the dark and ambient conditions without requiring any external energy or chemical.

4. Conclusions

In this study, Fe_2O_3/CNF was found to be active in degrading aromatic pollutants spontaneously under the dark and ambient conditions without using any external energy or chemical oxidant to assist the reaction. In particular, Fe_2O_3/CNF exhibited highly selective degradation activities for aromatic compounds. A spontaneous electron transfer from the aromatic compound (electron donor) to the Fe_2O_3/CNF (electron acceptor) initiates the oxidative degradation. Concurrently, ROS is generated by the sequential reduction of O_2 on the Fe_2O_3/CNF and facilitates the oxidation of aromatic compounds to achieve mineralization. The conventional Fenton-based processes using dissolved iron or iron oxide catalysts requires either H_2O_2 or external energy (*e.g.,* electricity in electro-Fenton, and light irradiation in photo-Fenton) to activate the pollutant decomposition. However, the present Fe_2O_3/CNF system enabled the spontaneous decomposition of aromatic compounds by activating O_2 under ambient condition. This catalytic oxidation system seems to be an ideal AOP with the following merits: (1) no toxic chemical oxidants (*e.g.,* O_3, H_2O_2, and Cl_2) are needed, (2) no external energy is required, (3) the reaction proceeds under ambient temperature and pressure conditions, (4) the catalyst material (Fe_2O_3/CNF) is low-cost and contains non-toxic elements and (5) the catalyst (in a sheet form) is easily handled and recoverable. The composite catalysts of Fe_2O_3 and carbon nanomaterials can be further developed as a more practical material for water treatment and environmental remediation.

Acknowledgments

This work was supported by “Next Generation Carbon Upcycling Project” (2017M1A2A2043123; 2017M1A2A2046736) and “the Global Research Laboratory (GRL) Program” (2014K1A1A2041044) through the National Research Foundation (NRF) and DGIST R&D program (17–NT–02) funded by the Ministry of Science and ICT, Republic of Korea.

Appendix A. Supplementary data

Supplementary material related to this article can be found, in the online version, at doi:https://doi.org/10.1016/j.apcatb.2019.118066.

References

[1] M. Mishra, D.-M. Chun, α-Fe_2O_3 as a photocatalytic material: a review, Appl. Catal. A : General 498 (2015) 126–141.
[2] J.-C. Wang, J. Ren, H.-C. Yao, L. Zhang, J.-S. Wang, S.-Q. Zang, L.-F. Han, Z.-J. Li, Synergistic photocatalysis of Cr(VI) reduction and 4-chlorophenol degradation over hydroxylated α-Fe_2O_3 under visible light irradiation, J. Harzard. Mater. 311 (2016) 11–19.
[3] Z. Zhang, M.F. Hossain, T. Takahashi, Self-assembled hematite (α-Fe_2O_3) nanotube arrays for photoelectrocatalytic degradation of azo dye under simulated solar light irradiation, Appl. Catal. B: Environ. 95 (2010) 423–429.
[4] D.A. Wheeler, G. Wang, Y. Ling, Y. Li, J.Z. Zhang, Nanostructured hematite: synthesis, characterization, charge carrier dynamics, and photoelectrochemical properties, Energy Environ. Sci. 5 (2012) 6682–6702.
[5] S.-S. Lin, M.D. Gurol, Catalytic decomposition of hydrogen peroxide on iron oxide: kinetics, mechanism, and implications, Environ. Sci. Technol. 32 (1998) 1417–1423.
[6] H.-H. Huang, M.-C. Lu, J.-N. Chen, Catalytic decomposition of hydrogen peroxide and 2-chlorophenol with iron oxides, Water Res. 35 (2001) 2291–2299.
[7] M. Hermanek, R. Zboril, I. Medrik, J. Pechousek, C. Gregor, Catalytic efficiency of iron(III) oxides in decomposition of hydrogen peroxide: competition between the surface area and crystallinity of nanoparticles, J. Am. Chem. Soc. 129 (2007) 10929–10936.
[8] F. Magalhães, M.C. Pereira, J.D. Fabris, S.E.C. Bottrel, M.T.C. Sansiviero, A. Amaya, N. Tancredi, R.M. Lago, Novel highly reactive and regenerable carbon/iron composites prepared from tar and hematite for the reduction of Cr(VI) contaminant, J. Hazard. Mater. 165 (2009) 1016–1022.
[9] Z. Ai, Z. Gao, L. Zhang, W. He, J.J. Yin, Core − shell structure dependent reactivity of Fe@Fe_2O_3 nanowires on aerobic degradation of 4-chlorophenol, Environ. Sci. Technol. 47 (2013) 5344–5352.
[10] Y. Mu, Z. Ai, L. Zhang, F. Song, Insight into core − shell dependent anoxic Cr(VI) removal with Fe@Fe_2O_3 nanowires: Indispensable role of surface bound Fe(II), ACS Appl. Mater. Inter. 7 (2015) 1997–2005.
[11] C. Joe-Wong, J. Gordon, E. Brown, K. Maher, Kinetics and products of chromium (VI) reduction by iron(II/III) bearing clay minerals, Environ. Sci. Technol. 51 (2017) 9817–9825.
[12] M.Y. Leiw, G.H. Guai, X. Wang, M.S. Tse, C.M. Ng, O.K. Tan, Dark ambient degradation of Bisphenol A and Acid Orange 8 as organic pollutants by perovskite $SrFeO_{3-\delta}$ metal oxide, J. Harzard. Mater. 260 (2013) 1–8.
[13] L.P. V, V. Rajagopalan, A new synergetic nanocomposite for dye degradation in dark and light, Sci. Rep. 6 (2016) 38606.
[14] S. Guo, G. Zhang, Y. Guo, J.C. Yu, Graphene oxide–Fe_2O_3 hybrid material as highly efficient heterogeneous catalyst for degradation of organic contaminants, Carbon 60 (2013) 437–444.
[15] S. Yun, Y.-C. Lee, H.S. Park, Phase-controlled iron oxide nanobox deposited on hierarchically structured graphene networks for lithium ion storage and photocatalysis, Sci. Rep. 6 (2016) 19959.
[16] T.-S. Kim, G.-H. Lee, S. Lee, Y.-S. Choi, J.-C. Kim, H.J. Song, D.-W. Kim, Carbon-decorated iron oxide hollow granules formed using a silk fibrous template: lithium-oxygen battery and wastewater treatment applications, NPG Asia Mater. 9 (2017) e450.
[17] M. Maiti, M. Sarkar, M.A. Malik, S. Xu, Q. Li, S. Mandal, Iron oxide NPs facilitated a smart building composite for heavy-metal removal and dye degradation, ACS Omega 3 (2018) 1081–1089.
[18] Y. Park, M. Oh, J.S. Park, S.-H. Baek, M. Kim, S. Kim, J.H. Kim, Electrochemically deposited Fe_2O_3 nanorods on carbon nanofibers for free-standing anodes of lithium-ion batteries, Carbon 94 (2015) 9–17.
[19] T.H. Jeon, G.-h. Moon, H. Park, W. Choi, Ultra-efficient and durable photoelectrochemical water oxidation using elaborately designed hematite nanorod arrays, Nano Energy 39 (2017) 211–218.
[20] H. Bader, V. Sturzenegger, J. Hoigne, Photometric method for the determination of low concentrations of hydrogen peroxide by the peroxidase catalyzed oxidation of N,N-diethyl-p-phenylenediamine (DPD), Water Res. 22 (1988) 1109–1115.
[21] A.P. Grosvenor, B.A. Kobe, N.S. McIntyre, Studies of the oxidation of iron by water vapour using X-ray photoelectron spectroscopy and QUASES, Surf. Sci. 572 (2004) 217–227.
[22] A.P. Grosvenor, B.A. Kobe, M.C. Biesinger, N.S. Mclntyre, Investigateion of multiplet splitting of Fe 2p XPS spectra and bonding in iron compounds, Surf. Interface Anal. 36 (2004) 1564–1574.
[23] M.C. Biesinger, B.P. Payne, A.P. Grosvenor, L.W.M. Lau, A.R. Gerson, R.S.C. Smart, Resolving surface chemical states in XPS analysis of first row transition metals, oxides and hydroxides: Cr, Mn, Fe, Co and Ni, Appl. Surf. Sci. 257 (2011) 2717–2730.
[24] M.S. Koo, K. Cho, J. Yoon, W. Choi, Photoelectrochemical degradation of organic compounds coupled with molecular hydrogen generation using electrochromic TiO_2 nanotube arrays, Environ. Sci. Technol. 51 (2017) 6590–6598.
[25] J. Lim, H. Kim, P.J.J. Alvarez, J. Lee, W. Choi, Visible light sensitized production of hydroxyl radicals using fullerol as an electron-transfer mediator, Environ. Sci. Technol. 50 (2016) 10545–10553.
[26] S.-H. Yu, D.E. Conte, S. Baek, D.-C. Lee, S.-K. Park, K.J. Lee, Y. Piao, Y.-E. Sung, N. Pinna, Structure-properties relationship in iron oxide-reduced graphene oxide nanostructures for Li-ion batteries, Adv. Funct. Mater. 23 (2013) 4293–4305.
[27] S. Trudel, E.D. Crozier, R.A. Gordon, P.S. Budnik, R.H. Hill, X-ray absorption fine structure study of amorphous metal oxide thin films prepared by photochemical metalorganic deposition, J. Solid State Chem. 184 (2011) 1025–1035.
[28] G. Kim, W. Choi, Charge-transfer surface complex of EDTA-TiO_2 and its effect on photocatalysis under visible light, Appl. Catal. B : Environ. 100 (2010) 77–83.
[29] G. Zhang, G. Kim, W. Choi, Visible light driven photocatalysis mediated via ligand-to-metal charge transfer (LMCT): an alternative approach to solar activation of titania, Energy Environ. Sci. 7 (2014) 954–966.
[30] Y.-H. Huang, Y.-J. Shih, C.-C. Chang, Adsorption of fluoride by waste iron oxide: the effects of solution pH, major coexisting anions, and adsorbent calcination temperature, J. Harzard. Mater. 186 (2011) 1355–1359.
[31] Y. Zhang, X. Lin, Q. Zhou, X. Luo, Fluoride adsorption from aqueous solution by magnetic core-shell Fe_3O_4@alginate-La particles fabricated via electro-coextrusion, Appl. Surf. Sci. 389 (2016) 34–45.
[32] J.T. Luo, Y.C. Yang, X.Y. Zhu, G. Chen, F. Zeng, F. Pan, Enhanced electrochemical response of Fe-doped ZnO films by modulating the chemical state and ionic size of the Fe dopant, Phys. Rev. B (2010) 014116.
[33] W. Wang, Y. Zhang, L. Wang, Y. Bi, Facile synthesis of Fe^{3+}/Fe^{2+} self-doped nanoporous $FeVO_4$ photoanodes for efficient solar water splitting, J. Mater. Chem. A (2017) 2478–2482.
[34] Y. Choi, M.S. Koo, A.D. Bokare, D.H. Kim, D.W. Bahnemann, W. Choi, Sequential process combination of photocatalytic oxidation and dark reduction for the rmoval of organic pollutants and Cr(VI) using Ag/TiO_2, Environ. Sci. Technol. 51 (2017) 3973–3981.

[35] G. Barzegar, S. Jorfi, V. Zarezade, M. Khatebasreh, F. Mehdipour, F. Ghanbari, 4-Chlorophenol degradation using ultrasound/peroxymonosulfate/nanoscale zero valent iron: Reusability, identification of degradation intermediates and potential application for real wastewater, Chemosphere 201 (2018) 370–379.
[36] W. Xiang, B. Zhang, T. Zhou, X. Wu, J. Mao, An insight in magnetic field enhanced zero-valent iron/H_2O_2 Fenton-like systems: critical role and evolution of the pristine iron oxides layer, Sci. Rep. 6 (2016) 24094.
[37] B.G. Anitha, L.G. Devi, Study of reaction dynamics of photocatalytic degradtaion of 4-chlorophenol using $SrTiO_3$, sulfur doped $SrTiO_3$, silver metallized $SrTiO_3$ and silver metallized sulfur doped $SrTiO_3$ catalysts: Detailed analysis of kinetic results, J. Surf. Interfaces Mater. 16 (2019) 50–58.
[38] J.C. Ma, D.A. Dougherty, The cation-π interaction, Chem. Rev. 97 (1997) 1303–1324.
[39] M. Wen, G. Li, H. Liu, J. Chen, T. An, H. Yamashita, Metal–organic framework-based nanomaterials for adsorption and photocatalytic degradation of gaseous pollutants: recent progress and challenges, Environ. Sci. Nano 6 (2019) 1006–1025.
[40] H. Jia, G. Nulaji, H. Gao, F. Wang, Y. Zhu, C. Wang, Formation and stabilization of environmentally persistent free radicals induced by the interaction of anthracene with Fe(III)-modified clays, Environ. Sci. Technol. 50 (2016) 6310–6319.
[41] X. Duan, Z. Ao, L. Zhou, H. Sun, G. Wang, S. Wang, Occurrence of radical and nonradical pathways from carbocatalyststsfor aqueous and nonaqueous catalytic oxidation, Appl. Catal. B : Environ. 188 (2016) 98–105.
[42] X. Duan, H. Sun, Z. Shao, S. Wang, Nonradical reactions in environmental remediation processes: Uncertainty and challenges, Appl. Catal. B : Environ. 224 (2018) 978–982.
[43] E.-T. Yun, J.H. Lee, J. Kim, H.-D. Park, J. Lee, Identifying the nonradical mechanism in the peroxymonosulfate activation process: singlet oxygenation versus mediated electron transfer, Environ. Sci. Technol. 52 (2018) 7032–7042.
[44] Y.-Y. Ahn, E.-T. Yun, J.-W. Seo, C. Lee, S.H. Kim, J.-H. Kim, J. Lee, Activation of peroxymonosulfate by surface-loaded noble metal nanoparticles for oxidative degradation of organic compounds, Environ. Sci. Technol. 50 (2016) 10187–10197.
[45] S. Lomnicki, H. Truong, E. Vejerano, B. Dellinger, Copper oxide-based model of persistent free radical formation on combustion-derived particulate matter, Environ. Sci. Technol. 42 (2008) 4982–4988.
[46] A.L.Nd. Cruz, W. Gehling, S. Lomnicki, R. Cook, B. Dellinger, Detection of environmentally persistent free radicals at a superfund wood treating site, Environ. Sci. Technol. 45 (2011) 6356–6365.
[47] G. Fang, J. Gao, C. Liu, D.D. Dionysiou, Y. Wang, D. Zhou, Key role of persistent free radicals in hydrogen peroxide actiation by biochar: Implications to organic contaminant degradation, Environ. Sci. Technol. 48 (2014) 1902–1910.
[48] B. Jiang, D. Dai, Y. Yao, T. Xu, R. Li, R. Xie, L. Chen, W. Chen, The coupling of hemin with persistent free radicals induces a nonradical mechanism for oxidation of pollutants, Chem. Commun. 52 (2016) 9566–9569.
[49] E.P. Vejerano, G. Rao, L. Khachatryan, S.A. Cormier, S. Lomnicki, Environmentally persistent free radicals: insights on a new class of pollutants, Environ. Sci. Technol. 52 (2018) 2468–2481.

Update

Applied Catalysis B: Environmental

Volume 269, Issue , 15 July 2020, Page

DOI: https://doi.org/10.1016/j.apcatb.2019.118231

Applied Catalysis B: Environmental 269 (2020) 118231

Contents lists available at ScienceDirect

Applied Catalysis B: Environmental

journal homepage: www.elsevier.com/locate/apcatb

Corrigendum

Corrigendum to "Ambient-temperature catalytic degradation of aromatic compounds on iron oxide nanorods supported on carbon nanofiber sheet" [Appl. Catal. B: Environ. 259 (2019) 118066]

Yiseul Park[a,1], Chuhyung Kim[b,1], Minsun Kim[c], Soonhyun Kim[c,*], Wonyong Choi[b,*]

[a] Department of Chemical Engineering, Pukyong National University, Busan, 48513, Republic of Korea
[b] Department of Chemical Engineering & Division of Environmental Science and Engineering, Pohang University of Science and Technology (POSTECH), Pohang, 37673, Republic of Korea
[c] Smart Textile Convergence Research Group, Daegu Gyeongbuk Institute of Science and Technology (DGIST), Daegu, 42988, Republic of Korea

The authors regret to inform that the following several errors in the aforementioned article.

(1) Missing asterisk mark for the co-corresponding author (**Dr. Soonhyun Kim**) in the online version of the article. It is essential that asterisk mark for the co-corresponding author.

(2) In abstract on page 1: "It is proposed that electrons spontaneously transfer from aromatic compound to O_2 viaFe_2O_3/CNF with initiating the oxidative degradation and the concurrent ROS generation." must be corrected to "It is proposed that electrons spontaneously transfer from aromatic compound to O_2 **via Fe_2O_3/CNF** with initiating the oxidative degradation and the concurrent ROS generation."

(3) In section 1. on page 1: "Recently, Fe/Fe_2O_3 composites have been used to degrade pollutants viaa reductive or oxidative pathway under dark conditions without additional reagents, but catalyst reuse and recovery were limited because of low catalytic property and stability [8–11]." must be corrected to "Recently, Fe/Fe_2O_3 composites have been used to degrade pollutants **via a** reductive or oxidative pathway under dark conditions without additional reagents, but catalyst reuse and recovery were limited because of low catalytic property and stability [8–11]."

(4) In section of 2.5. on Page 3: "Furthermore, the concentration of H_2O_2 was determined by using a DPD colorimetric method (based on the horseradish peroxidase-catalyzed reaction between H_2O_2 and DPD) using a UV–vis spectrophotometer (λ_{max} = 551 nm, ε = 21,000 M^1 cm) [20]." must be corrected to "Furthermore, the concentration of H_2O_2 was determined by using a DPD colorimetric method (based on the horseradish peroxidase-catalyzed reaction between H_2O_2 and DPD) using a UV–vis spectrophotometer (λ_{max} = 551 nm, **ε = 21,000 M^{-1} cm^{-1}**) [20]."

(5) In section 3.1. on page 3: "The average particle sizes of commercial iron oxides (*i.e.,* Fe_2O_3, FeOOH, and Fe_3O_4) used for the comparison of activity were 10–200 nm (Figs. 1–f)." must be corrected to "The average particle sizes of commercial iron oxides (*i.e.,* Fe_2O_3, FeOOH, and Fe_3O_4) used for the comparison of activity were 10–200 nm (**Figs. 1d–f**)."

(6) In section 3.2. on page 4: "It should be noted that the commercial iron oxides nanoparticles have widely varying sizes (*ca.* 10–200 nm, Figs. 1–f) but none of them exhibited any measurable activity for 4-CP oxidation." must be corrected to "It should be noted that the commercial iron oxides nanoparticles have widely varying sizes (*ca.* 10–200 nm, **Figs. 1d–f**) but none of them exhibited any measurable activity for 4-CP oxidation."

(7) In section 3.2. on page 4: "Although the significant deficit in the Cl mass balance indicates that there are a number of missing products and intermediates (Fig. S2), the apparent generation of Cl^- and 4-CC indicates that the observed 4-CP removal on Fe_2O_3/CNF did not occur viaasimple adsorption but by the 4-CP degradation." must be corrected to "Although the significant deficit in the Cl mass balance indicates that there are a number of missing products and intermediates (Fig. S2), the apparent generation of Cl^- and 4-CC indicates that the observed 4-CP removal on Fe_2O_3/CNF did not occur **via a simple** adsorption but by the 4-CP degradation."

(8) In section 3.2. on page 4: "However, when the degradation of 4-CP on Fe_2O_3/CNF was performed in N_2 saturated condition, where the oxidant generation viaO_2 reduction is not possible, the removal of 4-CP and the production of CO_2 were both negligible." must be corrected to "However, when the degradation of 4-CP on Fe_2O_3/CNF was performed in N_2 saturated condition, where the oxidant generation **via O_2** reduction is not possible, the removal of 4-CP and the production of CO_2 were both negligible."

(9) In caption of Fig. 3. on page 5: "(b) The production of chloride ions (Cl^-)and 4-CC from 4-CP (C_0 = 100 μM) degradation on Fe_2O_3/CNF (4 g L^{-1}; Total Cl = [4-CP] + [4-CC] + [Cl^-])." must be corrected to "(b) The production of chloride ions **(Cl-) and** 4-CC from 4-CP

DOI of original article: https://doi.org/10.1016/j.apcatb.2019.118066
* Corresponding authors.
E-mail addresses: sh2358@dgist.ac.kr (S. Kim), wchoi@postech.edu (W. Choi).
[1] These authors contributed equally to this work and should be considered co-first authors.

https://doi.org/10.1016/j.apcatb.2019.118231

Available online 27 February 2020

(C_0 = 100 μM) degradation on Fe_2O_3/CNF (4 g L^{-1}; Total Cl = [4-CP] + [4-CC] + [Cl^-])."

(10) In the caption of Fig. 5. on page 5: "(a) Fluorescence emission spectra evolution as a result of hydroxylated product formation via ˙OH reaction with TA (˙OH probe reagent) on Fe_2O_3/CNF." must be corrected to "(a) Fluorescence emission spectra evolution as a result of hydroxylated product formation **via ˙OH** reaction with TA (˙OH probe reagent) on Fe_2O_3/CNF."

(11) In section 3.5. on page 7: "The electron transfer was initiated from the aromatic compound (*i.e.,* 4-CP) to the Fe_2O_3/CNF, and the electrons were transferred to the CNF, and subsequently reduce O_2 to generate ˙OH viathe formation of $O_2^{\cdot -}$ and H_2O_2(Eqs. (1)–(4))." must be corrected to "The electron transfer was initiated from the aromatic compound (*i.e.,* 4-CP) to the Fe_2O_3/CNF, and the electrons were transferred to the CNF, and subsequently reduce O_2 to generate ˙OH **via the** formation of $O_2^{\cdot -}$ and **H_2O_2 (Eqs. (1)–(4))**."

(12) In section 3.5. on page 7: "It is consistent with the observation that Cl- and CO_2 were generated along with the degradation of 4-CP (*see* Figs. 3b and c)." must be corrected to "It is consistent with the observation that **Cl^-** and CO_2 were generated along with the degradation of 4-CP (*see* Figs. 3b and c)."

(13) In section 3.5. on page 8: "This spontaneous electron transfer process from an aromatic compound to PMS viacarbonaceous material can be similarly compared with that from an aromatic compound to O_2 viathe Fe_2O_3/CNF composite in this study." must be corrected to "This spontaneous electron transfer process from an aromatic compound to PMS **via carbonaceous** material can be similarly compared with that from an aromatic compound to O_2 **via the** Fe_2O_3/CNF composite in this study."

Above corrections do not change the overall results & discussion, and conclusion reported in the published article. The authors would like to apologise for any inconvenience caused.